Time-limited self-sustaining rhythms and state transitions in brain networks

Siyu Huo,[1] Yong Zou,[1] Marcus Kaiser,[2,3,4,*] and Zonghua Liu[1,†]

[1]*State Key Laboratory of Precision Spectroscopy and School of Physics and Electronic Science, East China Normal University, Shanghai 200241, P. R. China*

[2]*NIHR Nottingham Biomedical Research Centre, School of Medicine, University of Nottingham, Nottingham NG7 2UH, United Kingdom*

[3]*Sir Peter Mansfield Imaging Centre, University of Nottingham, Nottingham NG7 2RD, United Kingdom*

[4]*Rui Jin Hospital, Shanghai Jiao Tong University, Shanghai 200025, P. R. China*

(Received 15 June 2021; accepted 11 April 2022; published 27 April 2022)

Resting-state networks usually show time-limited self-sustaining oscillatory patterns (TLSOPs) with the characteristic features of multiscaled rhythms and frequent switching between different rhythms, but the underlying mechanisms remain unclear. To reveal the mechanisms of multiscaled rhythms, we present a simplified reaction-diffusion model of activation propagation to reproduce TLSOPs in real brain networks. We find that the reproduced TLSOPs do show multiscaled rhythms, depending on the activating threshold and initially chosen activating nodes. To understand the frequent switching between different rhythms, we present an approach of dominant activation paths and find that the multiscaled rhythms can be separated into individual rhythms denoted by different core networks, and the switching between them can be implemented by a time-dependent activating threshold. Further, based on the microstates of TLSOPs, we introduce the concept of a *return loop* to study the distribution of the return times of microstates in TLSOPs and find that it satisfies the Weibull distribution. Then, to check it for real data, we present a method of a shifting window to transform a continuous time series into a discrete two-state time series and interestingly find that the Weibull distribution also exists in resting-state EEG and fMRI data. Finally, we show that the TLSOP lifetime depends exponentially on the core network size and can be explained by a theory of the complete graphs.

DOI: 10.1103/PhysRevResearch.4.023076

I. INTRODUCTION

To perform various brain functions, the brain network has a unique small-world, modular, and hierarchical structure [1]. For efficiency, the brain network has been developed into different cognitive subnetworks, and each cognitive subnetwork is a group of interconnected regions functioning as a circuit and their collective dynamics may behave as a regular oscillation, i.e., the rhythms measured by electroencephalogram (EEG) data [2–4]. Thus, brain oscillation is highly rhythmic. Many experiments have confirmed the association between dominant brain rhythms and physiologic states. Different brain rhythms characterize distinct phases of the sleep-wake cycle [5,6]. For example, θ-band synchronization has been observed during lexical-semantic retrieval, indicating that θ synchronization supports the communication among distant cortical and subcortical regions which are involved in language [7–9]. The synchronization of α and β rhythms between right inferior frontal and primary sensory neocortex has been associated with attentional control [10]. And higher frequency γ rhythms in local synchronization have been observed during visual responses [11]. Further, it is revealed that even during sleep, we have a 90-min ultradian cycle, consisting of the repeated cycles of non-rapid-eye-movement and rapid-eye-movement sleep, ranging from states of deep unconsciousness to ordinary wakefulness [12,13].

Concerning dynamics, the performance of a cognitive task can be considered as the emergence of a dynamical pattern. Thus, understanding the dynamical patterns is a key to understanding the mechanism of rhythms. For this reason, many studies have been focused on the topic of self-sustained oscillations [14–16]. It is found that the existence of a self-sustained loop takes a key role for the rhythm and can be considered as a pacemaker loop [17–19]. This kind of oscillations by pacemaker loops is persistent and has a time-unlimited lifetime [20]. However, many signals by EEG data show that the lifetimes of cognitive patterns are generally not infinite but time-limited. Especially, this kind of time-limited patterns can be also produced by regional brain stimulations where the activated site will spread firing signal to its neighbors through the brain network structure and finally form different patterns of synchronization across predefined cognitive systems [21–24].

On the other hand, it is reported that the brain at rest displays spatial patterns of correlated activity across different brain areas known as resting-state networks (RSNs) with fewer links than during task performance [13,25]. The rhythm

*marcus.kaiser@nottingham.ac.uk
†zhliu@phy.ecnu.edu.cn

of RSNs will be frequently interrupted by the sleep-wake switch producing stable sleep and wakefulness, i.e., time-limited periods [26]. Thus, its two characteristic features are the multiscaled rhythms and frequent switching between different rhythms. Their mechanism may be essential for understanding the diversity of patterns in brain networks and help us to reveal fundamental principles for the organization of the human brain.

This switching may be more frequent during task states where the neurons in a network are rhythmically activated and inhibited. At one moment, many neuronal groups in our brain are active; while at another moment, other neuronal groups are active [27]. More examples can be found in pathologies such as epilepsy, autism spectrum disorders, schizophrenia, or Alzheimers disease, where there is frequent switching between diseases and normal states [28,29]. In this work, we present a framework to study the switching between brain oscillatory states. The framework is very simple and can be considered as a reaction-diffusion model where an inactivate node can be activated once its total input is greater than a given threshold. We first apply this model to a real brain network and find that different time-limited self-sustaining oscillatory patterns (TLSOPs) can be generated, depending on the initially activated nodes and chosen threshold. Then we analyze the rhythms contained in each TLSOP by presenting an approach of dominant activation paths. We find that the multiscaled rhythms can be separated into individual rhythms denoted by different core networks. Further, we present the concept of a return loop to study TLSOPs and find that the distribution of the return times of microstates satisfies the Weibull distribution and the TLSOP lifetime depends exponentially on the size of core network. After that, we present a shifting window approach to transform a continuous time series into a discrete two-state time series of $\{0, 1\}$ and confirm that a Weibull distribution also exists in real brain dynamics as observed in resting-state EEG and functional magnetic resonance imaging (fMRI) data. Finally, we present a theoretical analysis for the TLSOP lifetime, based on the complete graphs.

II. A SIMPLIFIED REACTION-DIFFUSION MODEL OF ACTIVATION PROPAGATION

It is well known that each brain neuron has two states, i.e., a quiescent or a firing state. The interaction between two neurons will take effect only when they are connected by a synapse. However, it is too difficult for us to directly consider this kind of coupling interaction on the neural level as the numbers of neurons and links in the human brain are enormous. To simplify this problem, we may make a coarse-grained description. A convenient way is to divide the cerebral cortex into different areas, i.e., regions of interest (ROIs). We let each ROI be a node and the density of synaptic connections between two ROIs be the weight of their link, and we thus obtain a weighted brain network. Depending on the precision of parcellation, we may obtain brain networks with different sizes N for a specific individual.

For such a brain network, a general way to study its dynamics is by letting each node be a neural oscillator such as the FitzHugh-Nagumo neuron or Hindmarsh-Rose neuron. However, this approach may be problematic as each node represents in fact the collective behaviors of thousands of neurons in a ROI, i.e., a mean field. For an isolated node with thousands of neurons, we may expect two kinds of behaviors, high or low firing rates. For the former, the total input coupling to each neuron in a ROI is sufficiently high to fire, thus making the neurons of ROIs insensitive to further input from other nodes. Consequently, the node may keep its state of high firing rate for a finite time. We call this state activation. While for the latter, the total input of each neuron in a ROI is insufficient to reach the threshold of firing, thus it is possible for the neurons of a ROI to receive input from other nodes. We call this state inactivation. Thus, for two connected nodes in brain network, their interaction can be approximately classified into three cases: (1) There is no interaction between them when both nodes are in the state of inactivation. (2) There is a firing transmission from the activated one to the inactivated one when one node is in the state of activation while the other is in the state of inactivation. The firing of an inactivated node depends on the total input received from all its neighbors. (3) The interaction will be small and can be ignored when both nodes are in the state of activation. However, in the case of a network, there can be a situation where input from multiple inactive nodes can result in the activation of multiple nodes as discussed in Refs. [30–32].

Based on this analysis, we here present a reaction-diffusion model. The model operates in discrete time steps and includes two steps: reaction and diffusion. The reaction step is only for the activated nodes and the diffusion step only for the inactivated nodes. Let $x_i(t)$ be the state of node i at time t. We assume $x_i(t) = 1$ for the activated node and $x_i(t) = 0$ for the inactivated node. In the reaction step, each activated node will have a probability p to become inactivated and $1 - p$ to remain in activated state. That is, we have

$$x_i(t+1) = \begin{cases} 0, & \text{with } p \\ 1, & \text{with } 1-p \end{cases} \tag{1}$$

for activated $x_i(t) = 1$. In the diffusion step, an inactivated node will become activated when its total input coupling strength is greater than a threshold w_c. The process can be represented as

$$x_i(t+1) = \Theta\left(\sum_{j=1}^{N} W_{ij} x_j(t) - w_c\right) \tag{2}$$

for inactivated $x_i(t) = 0$, where Θ denotes the Heaviside function.

Equations (1) and (2) constitute the simplified reaction-diffusion model of activation propagation. This model will go back to the threshold model of Ref. [33], provided that the weight matrix W_{ij} is replaced by the adjacency matrix M_{ij}.

Without loss of generality, we assume $p = 0.5$ in this work. Our purpose is to reveal the mechanism of the rhythms of human brain networks. For this purpose, we will focus on whether the initially activated nodes can make TLSOPs, by considering three kinds of real brain networks with different scales, i.e., small, middle, and large sizes, respectively.

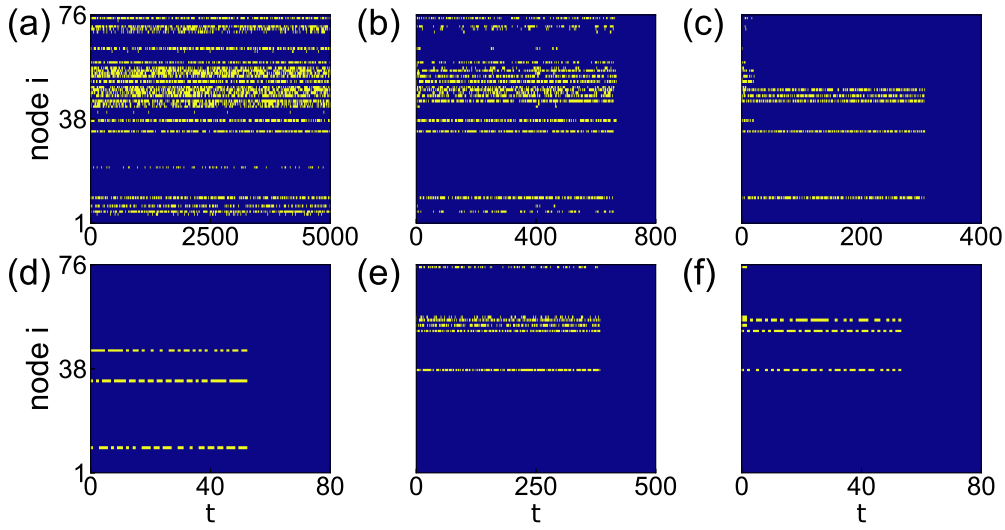

FIG. 1. Typical patterns by the reaction-diffusion model of Eqs. (1) and (2) where the "yellow" points represent $x_i(t) = 1$ and "blue" parts represent $x_i(t) = 0$. The threshold w_c is chosen as 0.006 in (a), 0.0068 in (b), 0.007 in (c), 0.009 in (d), 0.0066 in (e), and 0.009 in (f), and the initially activated nodes are chosen from the 76 nodes as follows: randomly choose 10 nodes in (a), choose the 14 nodes ([45−58]) in (b) and (c), choose the three nodes 10, 34, 45 in (d), and choose the six nodes 38, 52, 54, 75, 56, 57 in (e) and (f).

III. RESULTS

A. Time-limited self-sustaining oscillatory patterns

In numerical simulations, we here show only the results on the network with small scale and leave the results on the networks of both middle and large sizes in the Supplemental Material (SM) [34]. For the network with small scale, we take the structural connectivity from Refs. [21,35,36] as an example, which consists of 76 nodes (brain regions) across nine cognitive systems (resting-state networks). Each cognitive system is defined by regions that coactivate in support of a generalized class of cognitive functions, and the nine cognitive systems are named attention, auditory, cingulo-opercular, frontoparietal, medial default mode, motor and somatosensory, subcortical, ventral temporal association, and visual systems, respectively. A node of each cognitive network contains about ten ROIs and thus represents a brain region [21,36]. As different nodes represent different brain regions, the interconnections between them will be significantly different, resulting in weighted network edges based on structural connectivity between brain regions. Therefore, we have to consider different W_{ij} in Eq. (2). As this network is constructed by the cognitive functions, it may direct us to deeply understand the time-limited self-sustaining patterns in brain networks. These data of link weights W_{ij} can be taken from Ref. [35], which come from whole-brain fiber tractography and are measured by diffusion MRI analysis [21]. In the resulting weighted matrices, W_{ij} reflects the density of streamlines connecting different regions, i.e., normalized by the sum of the regional brain volumes. There are 30 subjects in the data, i.e., 30 networks. Our numerical simulations show that all the networks have similar results, thus we randomly take one from them, subject 13, and show the results of other subjects in the SM [34]. We first study the evolutionary processes of Eqs. (1) and (2) by choosing different initially activated nodes and different thresholds. We find that there are a variety of dynamical patterns, including both the self-sustained patterns and TLSOPs or both the stable and metastable states. Figures 1(a)–1(f) show six typical patterns, where Fig. 1(a) represents the case of self-sustained patterns and Figs. 1(b)–1(f) the case of TLSOPs. Moreover, we notice that in each panel of Fig. 1 the firings from different channels are sequential or alternative during the evolutionary process, i.e., the time series of firings in each channel is not continuous but with a blank from time to time. In this sense, the firings will run among the channels and form a limit-cycle-like behavior.

The threshold w_c in Eq. (2) is a key parameter to influence the types of patterns. Obviously, a zero threshold (i.e., $w_c = 0$) will always make $x_i(t+1) = 1$, i.e., producing a time-unlimited pattern, while too large of a threshold will always make $x_i(t+1) = 0$, i.e., producing no patterns. Thus, the thresholds for Fig. 1 are chosen by the conditions that Fig. 1(a) is a time-unlimited self-sustaining oscillatory pattern while Figs. 1(b)–1(f) are TLSOPs. That is, the thresholds for Figs. 1(b)–1(f) should not be too small or too large so as to avoid either the time-unlimited oscillatory pattern or no oscillatory pattern. We focus on the cases of Figs. 1(b)–1(f) and summarize three conclusions: (1) Let T be the lifetime for a TLSOP to survive. We see that T is significantly different from Figs. 1(b) to 1(f), indicating the feature of finite time. (2) Comparing Fig. 1(c) with Fig. 1(d) and Fig. 1(e) with Fig. 1(f), respectively, we find that Fig. 1(d) is contained in Fig. 1(c) and Fig. 1(f) is contained in Fig. 1(e), indicating the feature of multiscaled rhythms. And (3) comparing Figs. 1(c) and 1(e) with Fig. 1(b), we see that both Figs. 1(c) and 1(e) are contained in Fig. 1(b), indicating that multiple rhythms can be contained in a single TLSOP, i.e., in Fig. 1(b). Thus, it will result in a switching between different rhythms when the activated nodes change from one rhythm to the other.

Do the results of Fig. 1 depend on the parameter p of Eq. (1)? To figure out the answer, we have made numerical simulations for different p and found the similar results, indicating that the existence of TLSOPs is robust to p. We have

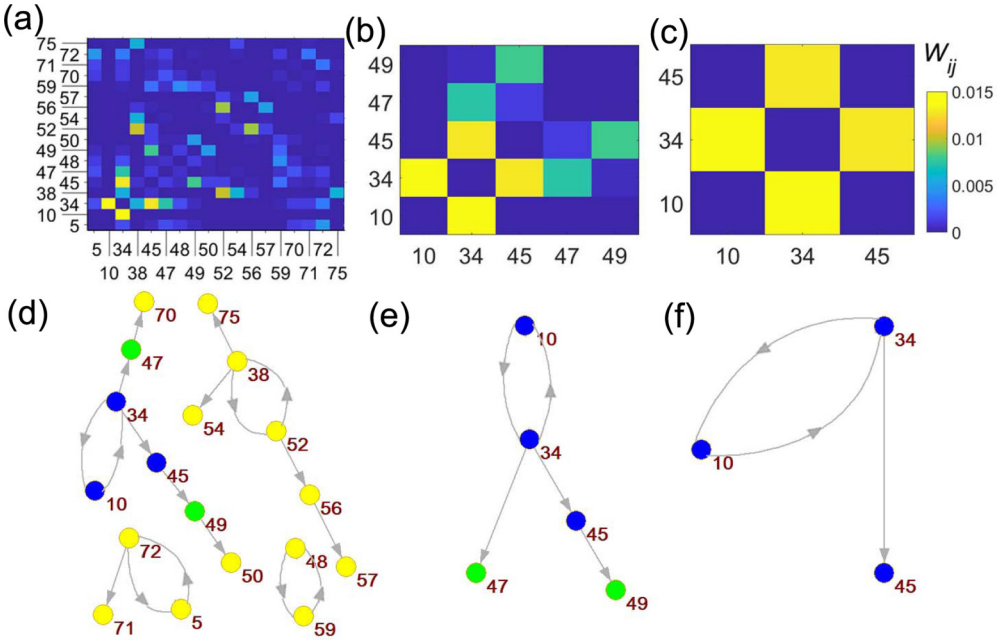

FIG. 2. Application of the approach of dominant activation paths to the three cases of Figs. 1(b)–1(d), where there are 18 nodes in (a), five nodes in (b), and three nodes in (c). Panels (a)–(c) represent the weight matrix W_{ij} of connections for *the core networks* of self-sustained patterns, corresponding to Figs. 1(b)–1(d), respectively. Panels (d)–(f) represent *the dominant activation paths* for the self-sustained pattern, corresponding to (a)–(c), respectively.

shown the results of $p = 0.3$ and 0.8 in Figs. 2 and 3 of the SM [34]. Thus, here we fix $p = 0.5$ in this work.

Do these three conclusions imply some basic principles hidden in TLSOPs? To figure out the answer, we will develop several approaches in the following subsections.

B. An approach of dominant activation paths to identify individual TLSOP rhythms

As all the TLSOPs of Figs. 1(c) to 1(f) are contained in Fig. 1(b), an interesting question will be how can we identify them directly from Fig. 1(b)? In other words, suppose we have only the time series of Fig. 1(b), can we recognize its individual rhythms? To answer this question, we here present an approach of dominant activation paths to study the rhythms contained in TLSOPs, as the patterns observed in experiments are time-limited [5–9,26]. We will show that the rhythms can be represented by corresponding core networks with different sizes.

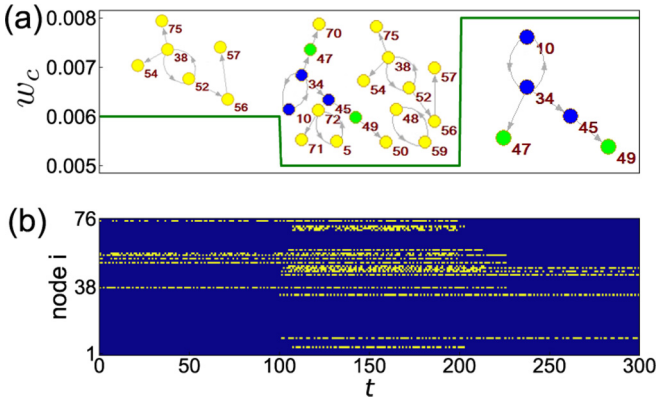

FIG. 3. Implementing the switching between different TLSOP rhythms by a time-dependent threshold. (a) Time-dependent threshold w_c where the threshold w_c is chosen as 0.006 for $t < 100$, 0.005 for $100 < t < 200$, and 0.008 for $200 < t < 300$, respectively. The insets show their corresponding dominant activation paths, respectively. (b) The evolutionary process of the TLSOP patterns where the threshold w_c is changed according to (a).

To illustrate our idea, we take the TLSOPs of Figs. 1(b)–1(d) as an example, which contain 18 nodes in Fig. 1(b), five nodes in Fig. 1(c), and three nodes in Fig. 1(d). Figures 2(a)–2(c) show the final weight matrix W_{ij} of connections for the subnetworks of self-sustained patterns, i.e., *the core networks*, corresponding to Figs. 1(b)–1(d), respectively, where the numbers denote the node numbers in the brain network and the colors denote the values of W_{ij}. Three features can be noticed from Figs. 2(a)–2(c): (1) By the node numbers we see that the nodes in each TLSOP are not chosen sequentially from the original order $1, 2, \ldots, 76$ in Fig. 1, but are noncontinuous at intervals such as 10, 45, and 34 in Fig. 2(c); (2) all three subnetworks are complete graphs but with different connection weights; and (3) Fig. 2(b) is contained in Fig. 2(a) and Fig. 2(c) is contained in Fig. 2(b). Do these features imply some basic principles hidden in the self-sustained patterns? If so, the finding of these principles will definitely help us to understand the rhythms of brain waves and may further help us to control and regulate the rhythms in brain disorders.

To answer this question, we recall the method of dominant phase-advanced driving (DPAD) [37,38], which has revealed that the existence of a DPAD loop is a key feature for a self-sustained pattern [17–20]. In this method, the key point is to figure out a loop of connected nodes where each nonoscillatory node can oscillate if and only if it is driven by one or

few oscillatory interactions with advanced phases. Once this DPAD loop is determined, the oscillations of this loop will be constantly transmitted to other nodes and thus form a periodic self-sustained pattern. In this sense, the DPAD loop will behave as a pacemaker and determine the period of the self-sustained oscillation. However, we notice from Figs. 1(b)–1(f) that these TLSOPs are not periodic but irregular, thus we cannot use the approach of a DPAD loop. To solve this problem, we here introduce an approach for TLSOPs, based on the spirit of DPAD. In detail, we introduce an activation matrix M with its element M_{ij} representing the frequency of activated link $j \to i$. Initially, we let all the elements of M be zero, $M_{ij} = 0$. For an evolutionary process related to the node i and its one neighboring node j, if $x_i(t-1) = 0$ and $x_i(t) = 1$, the link $j \to i$ will be considered as an activated link for one time step and $M_{ij} = M_{ij} + W_{ij}$, provided $x_j(t-1) = 1$. In this way, we can get the accumulated M_{ij} for a time period. For each node i in the self-sustained pattern, we pick out the maximum M_{ij} from all its neighboring M_{ij}, i.e., the dominant one. Then we put a directional link from the dominant node j to the node i. In this way, every node in TLSOPs will have one dominant node j and thus only one incoming link. All these incoming links will form the most significant driving paths for TLSOPs. We would like to call them *the dominant driving paths* as they are based on the statistical frequencies of activations but not the interaction providing the most significant activating contribution at a time step as in [37,38]. If some of these incoming links form a loop, it will be the loop of dominant activation path. Figures 2(d)–2(f) show the results, corresponding to Figs. 2(a)–2(c), respectively. We do see that there is at least one loop of dominant activation paths in each of Figs. 2(d)–2(f), where the loop is the core topology for the oscillation serving as the source loop and the unidirectional links indicate the firing propagation pathways. Therefore, the loop of dominant activation path significantly simplifies the connection subnetwork and shows the main flow direction of firing propagation.

Further, we notice from Fig. 2(d) that its loops of dominant activation paths are not an entity but separated into four parts, where each part has an independent loop. In fact, each separated part also can be considered as connected components of dominant activation paths as it can make a self-sustained oscillation by its loop. We would like to call its connection network the *core network*, with the loop being its hallmark. As the four parts have different sizes, their rhythms will be different and thus make multiscaled TLSOP rhythms, i.e., the mechanism of multiscales. Take the upper-left part of Fig. 2(d) as an example. It consists of seven nodes, but its loop consists of only two nodes, i.e., the two nodes 10 and 34. As this loop behaves like a pacemaker, the upper-left part of Fig. 2(d) can have a sustained oscillation. To confirm its independence to other three parts of Fig. 2(d), Fig. 2(e) shows the TLSOP from partial nodes of the upper-left part of Fig. 2(d) but with the loop. Figure 2(f) further shows the case from partial nodes of Fig. 2(e) but also with the loop. We see from both Figs. 2(e) and 2(f) that the self-sustained patterns can survive, provided that the loop exists. Thus, the self-sustained pattern of Fig. 2(a) is contributed by four core networks.

We have to emphasize that all the sustained activity patterns always have at least one loop in M_{ij}, which has been confirmed in all our simulations. The reason is that each TLSOP has a finite lifetime and thus needs recycles of firing propagation. Considering the fact that each node in *the dominant driving paths* has only one incoming link, thus a core network will be a directional tree if there is no loop in M_{ij}. In this case, the recycles of firing propagation cannot be implemented.

C. How to implement the switching between different TLSOP rhythms

Based on the individual TLSOP rhythms identified in Sec. III B, a key question is how to implement the switching between them. To solve this problem, we start from the network of Fig. 2(a), which is a fully connected network with the weight matrix W_{ij} from Refs. [21,35,36]. By letting the threshold w_c be time-dependent, we find that the switching between different TLSOP rhythms can be implemented. Figure 3 shows such an example where the variation of w_c is given in Fig. 3(a) and the corresponding TLSOP patterns are given in Fig. 3(b). From Fig. 3(b) we see that it is a pattern of six nodes for $t < 100$, 18 nodes for $100 < t < 200$, and five nodes for $200 < t < 300$, indicating that the switching between different TLSOP rhythms has been implemented by a time-dependent activating threshold. In detail, the insets of Fig. 3(a) show their corresponding dominant activation paths, respectively. We see that the middle part is the whole of Fig. 2(d), while both the left and right parts are only the subsets of the middle part. From these insets we also see that each of the left and right patterns has a unique rhythm and the middle pattern has a multiple rhythms; thus the changing of TLSOP patterns in Fig. 3(b) represents the switching between different rhythms of TLSOP. This may be one way to implement the switching between different TLSOP rhythms, but other ways are also possible.

D. Statistics of TLSOP microstates by a return-loop approach

To make the study more detailed, we would like to figure out the basic principles hidden in TLSOPs of Fig. 1. For this purpose, we present a concept of *return loop* to study TLSOP microstates. For a TLSOP, such as the ones of Figs. 1(b)–1(f), we find that there are many different microstates during the evolutionary process and each specific microstate will show up from time to time. That is, we have only one microstate at each time step but different microstates at different time steps. To understand how the macroscopic rhythms come from these microstates, we introduce a variable $\mathbf{S}$ to represent the microstate, which is a m-dimensional vector with m being the number of nodes in a TLSOP. Take the TLSOP of Fig. 1(c) as an example. Its m equals 5. As the time series of each node consists of 0 and 1, $\mathbf{S}$ will take the following forms: (1, 1, 1, 1, 1), (1, 0, 1, 1, 0), (0, 1, 0, 0, 1), and so on. Taking off the microstate (0,0,0,0,0) of death, we have a total of $2^m - 1$ different microstates, i.e., 31 for $m = 5$. For convenience, we rename these microstates $S1$, $S2$, $S3$, and so on. In a TLSOP, these microstates will recurrently appear many times. There will be a return loop once a specific microstate shows up two consecutive times. Take the microstate $S1$ as an example. We will have a return loop once the system

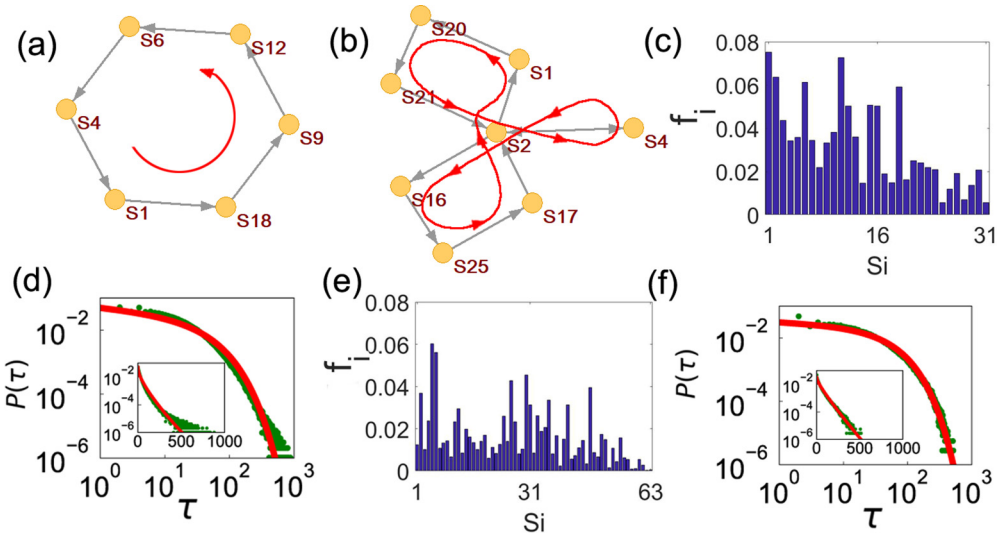

FIG. 4. The approach of the return loop. Panels (a) and (b) represent two typical TLSOP return loops in Fig. 1(c) with $m = 5$, based on the return of $S1$. Panel (c) represents the frequencies of TLSOP microstates $Si(i = 1, 2, \ldots, 31)$ in Fig. 1(c). Panel (d) represents the TLSOP distribution of τ from Fig. 1(c) with 1000 realizations with the same initial activated nodes, where the red line is produced by the Weibull distribution with $\lambda = 30$, $\beta = 0.8$, and $C = 1$. Panels (e) and (f) are from the TLSOP of Fig. 1(e) with $m = 6$ where the red line in (f) is produced by the Weibull distribution with $\lambda = 41$, $\beta = 0.9$, and $C = 1$.

goes back to $S1$. Figures 4(a) and 4(b) show two typical return loops based on the return of $S1$, respectively.

Let τ be the return time from a microstate Si to its first return, i.e., the length of a return loop. Two features can be found from Figs. 4(a) and 4(b). The first one is that only part of all the microstates appear in each return loop, indicating that different Si will have different possibilities to appear in individual return loops. Let f_i be the frequency for Si to appear in all the individual return loops, i.e., the possibility for Si to appear in the TLSOP evolutionary process. Figure 4(c) shows all the frequencies f_i of $Si(i = 1, 2, \ldots, 31)$ from the TLSOP of Fig. 1(c). We see that some f_i are large but others are small, implying that some microstates are dominant. The second one is that τ are different in Figs. 4(a) and 4(b), indicating that the return times of Si are not constant. That is, we may have many different τ during the TLSOP evolution. For the same reason, we also have many different τ for other Si during TLSOP the evolution. Collecting all these τ from different Si arises a question: Do these τ satisfy a distribution related to brain functions? This question is not trivial as a stable distribution represents the statistics contained in system, i.e., frequency heterogeneity of different microstate Si. To figure out the answer, we notice that there is a specific microstate Si at each TLSOP time step and a corresponding τ can be obtained, provided that we can find the next Si. In this way, we can find all the τ of TLSOPs. As a TLSOP is time-limited, we may not have enough τ for statistics. To solve this problem, we do 1000 realizations to obtain enough τ by choosing the same initial activated nodes. Figure 4(d) shows the distribution of τ in a log-log plot and the inset shows it in a log-linear plot. We see that both are not straight lines, indicating that it is neither a power-law nor an exponential distribution.

Recalling that a TLSOP is a transient process between the permanent oscillation and oscillation death, we assume that it represents the status of brain at criticality. It is well known that there is a self-organized criticality in equilibrium systems, leading to emergent collective behavior across scales, i.e., power laws [39]. Whereas in nonequilibrium systems, the Weibull distribution is used extensively to model heterogeneous distribution of events [40], such as the δ-burst durations in the sleep-wake cycle [41]. As a TLSOP is a typical nonequilibrium state, we here use the Weibull distribution to fit the data of Fig. 4(d), described as $P(\tau, \beta, \lambda, C) = C(\frac{\beta}{\lambda})(\frac{\tau}{\lambda})^{\beta-1}e^{(\frac{\tau}{\lambda})^{\beta}}$ where λ is the characteristic timescale, β the shape parameter, and C the fitting factor. The red line in Fig. 4(d) is produced by the Weibull distribution with $\lambda = 30$, $\beta = 0.8$, and $C = 1$. We see that the red line fits the data very well, implying that the distribution of τ satisfies the Weibull distribution. These two features can be further confirmed by the TLSOP of Fig. 1(e) with $m = 6$; see Figs. 4(e) and 4(f), respectively. More results for other subjects are shown in the SM [34].

E. TLSOPs of fMRI data by a shifting window approach

It will be of great interest if the above findings can be supported by real time series. As the reaction-diffusion model of (1) and (2) describes only the activation propagation of initial activated nodes but does not consider any cognitive tasks, its dynamical patterns may correspond to the dynamics of RSNs, which are especially important in exploring the basic principles of self-organizing brain dynamics [13,42]. For this purpose, we here consider the case of fMRI data from RSNs, but leave the discussion on the case of the EEG data to the SM [34].

We consider the public fMRI data of RSNs from Ref. [43], which consist of 99 healthy participants. For each subject, 90 time series are measured from its 90 brain regions, i.e., one time series from one brain region. We calculate the Pearson correlation coefficient between any two of these 90 time series to obtain a weight matrix. Then we set a threshold to obtain the functional brain network [44]. When the threshold is large, the

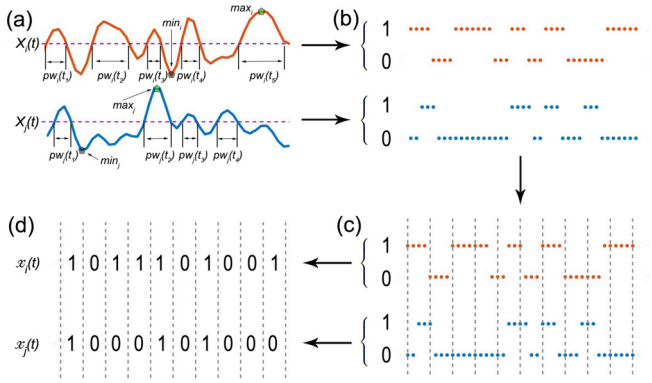

FIG. 5. Schematic figure for the approach of *shifting window*. Panel (a) represents two arbitrary time series and the calculating of the peak width $pw_i(t)$. Panel (b) represents the transformation of continuous time series to a discrete time series. Panel (c) represents the partition of the discrete time series by a shifting window. Panel (d) represents the final results of a discrete time series.

obtained network will not be a connected one but fragmented with local clusters. Figures 6(a)–6(c) below show three such clusters from subjects 1, 7, and 16, respectively. More examples are given in the SM [34]. We assume that the dynamics of these clusters correspond to the TLSOPs of Figs. 1(b)–1(f). However, we face a problem that the fMRI data are continuous time series, while those by Eqs. (1) and (2) are discrete time series consisting of 0 and 1. To overcome this problem, we have to transform the fMRI data into a discrete time series of $\{0, 1\}$. A general way to do this is by simply asking at each time point whether a region is more or less active than its average, which yields binary time series with the same lengths as the original data [45]. Using this approach to the fMRI data of Fig. 5(a), we will have consecutive 1 for the part larger than the average and consecutive 0 for the part less than the average, resulting in highly correlated signals in close time points. Thus, this approach will not increase the effective number of samples. For this aspect, we here introduce an approach of a *shifting window*, which is shown in Fig. 5 and consists of the following steps:

(1) For a continuous time series $X_i(t)$, we first find its maximum $X_i^{\max}$ and minimum $X_i^{\min}$ and then let their average be the threshold X_{th}, i.e., $X_{th} = (X_i^{\max} + X_i^{\min})/2$. See Fig. 5(a).

(2) Calculate all the peak widths above the threshold by $pw_i(t_1) = t_2 - t_1$, with t_1 and t_2 being two consecutive times crossing the threshold X_{th}, i.e., $X_i(t_1) < X_{th}$ and $X_i(t_1 + 1) > X_{th}$ and $X_i(t_2) > X_{th}$ and $X_i(t_2 + 1) < X_{th}$. The average peak width will be $Pw_i = \langle pw_i(t_1)\rangle_{t_1}$. See Fig. 5(a).

(3) Calculate Pw_j for all the other time series j in the connected cluster and choose the minimum of them as our shifting window Pw, i.e., $Pw = \min\{Pw_1, Pw_2, \ldots\}$.

(4) Transform all the continuous time series $X_i(t)$ into a discrete time series $X_i'(t)$ by letting $X_i'(t) = 1$ when $X_i(t) > X_{th}$, and $X_i'(t) = 0$ otherwise. In this way, there will be many consecutively 0 or 1 in $X_i'(t)$. See Fig. 5(b).

(5) Finally, we use a shifting window to consecutively cover $X_i'(t)$ and let $x_i(t)$ denote the value of the window i, which will be either 1 or 0. In detail, we let n_0 and n_1 be the numbers of $X_i'(t) = 0$ and $X_i'(t) = 1$ in the window i, respectively, and let the majority of the two numbers be the value of $x_i(t)$, i.e., $x_i(t) = 0$ if $n_0 > n_1$, and $x_i(t) = 1$ otherwise. See Figs. 5(c) and 5(d).

By these steps, a continuous time series $X_i(t)$ will be transformed into a discrete time series $x_i(t)$ of $\{0, 1\}$, but the length of $x_i(t)$ will be compressed to $1/pw$ of $X_i(t)$. Now, $x_i(t)$ corresponds to the discrete time series of Eqs. (1) and (2) and thus can be used to check our findings.

Taking Fig. 6(a) as an example and doing the same procedure as in Fig. 4(d) and 4(f), Fig. 6(d) shows the distribution of τ for the TLSOP of Fig. 6(a), where the red line is the fitted curve by the Weibull distribution with $\lambda = 5$, $\beta = 0.95$, and $C = 1.2$. We see that it fits very well with the data, indicating that the result of the fMRI data has confirmed the result from the model of Eqs. (1) and (2). This conclusion has been further

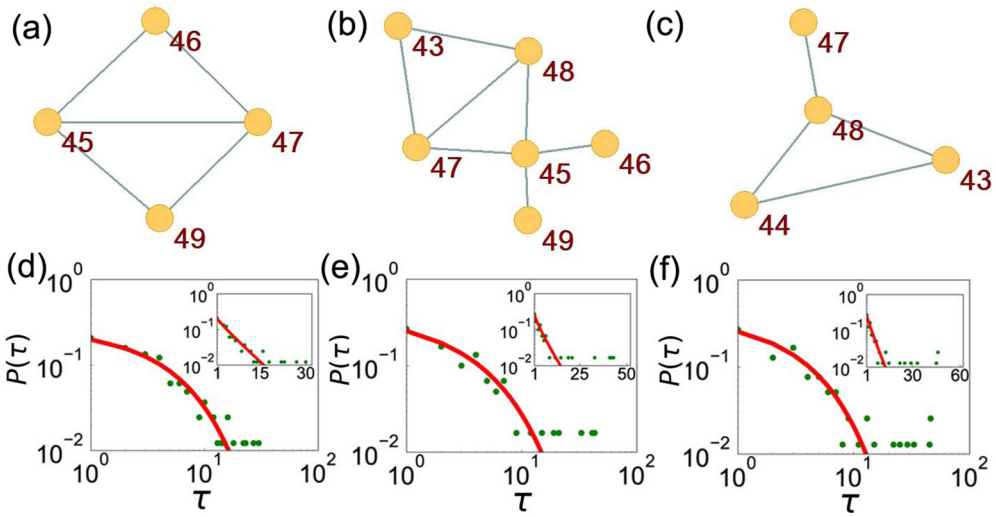

FIG. 6. The core TLSOP networks and their corresponding distributions of τ for the fMRI data. Panels (a)–(c) represent three core networks from the subjects 1, 7, and 16, respectively. Panels (d)–(f) correspond to (a)–(c), respectively, where the red lines are the fitted curves by the Weibull distribution with $\lambda = 5$, $\beta = 0.95$, and $C = 1.2$ in (d), $\lambda = 4$, $\beta = 0.9$, and $C = 1.3$ in (e), and $\lambda = 3.5$, $\beta = 0.95$, and $C = 1.2$ in (f).

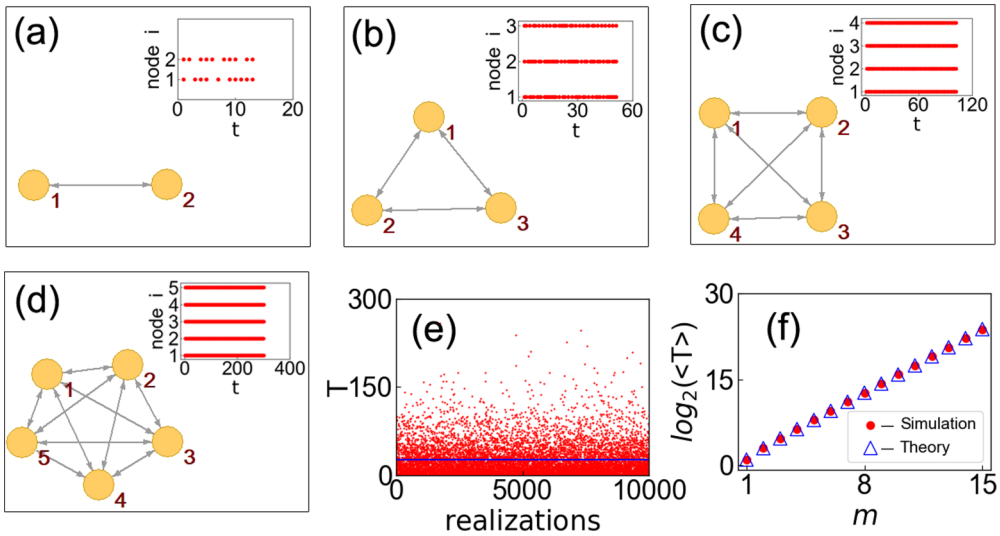

FIG. 7. Relationship between lifetime T and core network for $w = 0.08$ and $w_c = 0.07$. Panels (a)–(d) represent the core networks and their TLSOPs (i.e., the insets) for $m = 2, 3, 4$, and 5, respectively. Panel (e) represents T for different realizations for the case of (b) where the straight line denotes the average $\langle T \rangle$. Panel (f) represents the relationship between $log_2\langle T \rangle$ and m for $m = 1, 2, \ldots, 15$, where the "circles" and "triangles" denote the results from numerical simulations and theoretical analysis, respectively.

confirmed by Fig. 6(e) for the TLSOP of Fig. 6(b) and Fig. 6(f) for the TLSOP of Fig. 6(c).

We have also consider the EEG data of RSNs from Ref. [46], which comprises 18 healthy participants and each with 128 time series. Our results show that it is similar to the case of fMRI data; see the SM [34] for details.

F. A brief theoretical analysis

In general, for a stochastic differential equation, the master equation formalism is a good choice to make a theoretical analysis. However, because of the nonlinear Heaviside function of Θ in Eq. (2), it is difficult for us to use the master equation formalism. In this sense, we here would like to choose an alternative approach to make a theoretical analysis.

We notice from Figs. 1(b)–1(f) that their lifetimes T are different from each other and also notice that their final patterns are stable and are not exactly the initially activated nodes. Take Fig. 1(c) as an example. Its final pattern consists of five nodes, which is much less than the 14 initially activated nodes. Further, by checking the network connections we find that the final pattern of the five nodes is a complete graph, i.e., a core network. We have confirmed the existence of a single core network in Figs. 1(c)–1(f) and multiple core networks in Fig. 1(b). Thus, T is closely related to the core TLSOP networks. To figure out the relationship between T and core network, we here design four core networks with two, three, four, and five nodes, respectively; see Figs. 7(a)–7(d). We let all the links have the same weight w and let w be slightly greater than the threshold w_c. The insets of Figs. 7(a)–7(d) show their TLSOPs, respectively. We see that the lifetime T continuously increases from Fig. 7(a) to 7(d), implying more nodes in a core network and longer T. Considering the randomness in making the lifetime, we make a large number of realizations and take their average $\langle T \rangle$. Take the case of Fig. 7(b) as an example. Figure 7(e) shows its T for different realizations, with the average $\langle T \rangle \approx 26.01$ (see the straight line). By this way, we can get $\langle T \rangle$ for core networks with different numbers of nodes, i.e., m. The "circles" in Fig. 7(f) show the results for the relationship between $\log_2\langle T \rangle$ and m.

To present a theoretical analysis to the observed results in Fig. 7, we here focus on some specific TLSOP core networks, i.e., those complete graphs with m nodes. We let the weights of all the links be slightly greater than the threshold w_c. More specifically, we let $\langle T \rangle$ be the average lifetime when all the m nodes are initially activated, i.e., with initial state of $(1, 1, \ldots, 1)$. When $m = 1$, the only activated node will have the possibility p to become inactivated, thus its lifetime will be $\langle T \rangle = 1/p$. For the case of $p = 1/2$, we have $\langle T \rangle = 2$.

When $m = 2$, Fig. 7(a) shows its TLSOP core network. For the two nodes 1 and 2, there are three possible initial activation states 01, 10, and 11, and each of them may have four possible outputs 00, 01, 10, and 11. Following Eqs. (1) and (2), Table I shows the probabilities of the four outputs from each initial activation state, where the first line represents the three initial activation states and the first column denotes the four possible outputs.

Let the average lifetimes of the initial activation states 01, 10, and 11 be y_1, y_2, and y_3, respectively. We will have

$$y_1 = p(y_2 + 1) + (1 - p)(y_3 + 1) \tag{3}$$

where the first term $p(y_2 + 1)$ represents the lifetime for the initial state 01 to become 10 and the second term $(1 - p)(y_3 +$

TABLE I. The initial activation states of Fig. 7(a) vs their outputs.

State	01	10	11
00	0	0	p^2
01	0	p	$p(1-p)$
10	p	0	$p(1-p)$
11	$1-p$	$1-p$	$(1-p)^2$

TABLE II. The initial activation states of Fig. 7(b) vs their outputs.

State	001	010	100	011	101	110	111
000	0	0	0	0	0	0	p^3
001	0	0	0	0	0	p^2	$p^2(1-p)$
010	0	0	0	0	p^2	0	$p^2(1-p)$
100	0	0	0	p^2	0	0	$p^2(1-p)$
011	0	0	p	0	$p(1-p)$	$p(1-p)$	$p(1-p)^2$
101	0	p	0	$p(1-p)$	0	$p(1-p)$	$p(1-p)^2$
110	p	0	0	$p(1-p)$	$p(1-p)$	0	$p(1-p)^2$
111	$1-p$	$1-p$	$1-p$	$(1-p)^2$	$(1-p)^2$	$(1-p)^2$	$(1-p)^3$

1) for the initial state 01 to become 11. In the same way, we may have

$$y_2 = p(y_1+1) + (1-p)(y_3+1) \tag{4}$$

and

$$y_3 = p^2 + p(1-p)(y_1+1) + p(1-p)(y_2+1) + (1-p)^2(y_3+1). \tag{5}$$

The solutions of Eqs. (3)–(5) can be obtained as $y_1 = y_2 = \frac{1+p-p^2}{p^2(1-p)}$ and $y_3 = \frac{1+2p}{p^2}$. For the case of $p = 1/2$, we have $y_1 = y_2 = 10$ and $y_3 = 8$. As y_3 represents the case of all the initially activated m nodes, we have $\langle T\rangle = y_3 = 8$, which is consistent with Fig. 7(f).

Then we consider the motif of Fig. 7(b). For the three nodes 1–3, there are seven possible initial activation states 001, 010, 100, 011, 101, 110, and 111, and each of them may have eight possible outputs 000, 001, 010, 100, 011, 101, 110, and 111. Table II shows the probabilities for each initial activation, where the first line represents the seven initial activation states and the first column denotes the eight possible outputs.

Let the average lifetimes of the initial activation states 001, 010, 100, 011, 101, 110, and 111 be $y_1, y_2, y_3, y_4, y_5, y_6$, and y_7, respectively. We will have

$$\begin{aligned}
y_1 &= p(y_6+1) + (1-p)(y_7+1),\\
y_2 &= p(y_5+1) + (1-p)(y_7+1),\\
y_3 &= p(y_4+1) + (1-p)(y_7+1),\\
y_4 &= p^2(y_3+1) + p(1-p)(y_5+1)\\
&\quad + p(1-p)(y_6+1) + (1-p)^2(y_7+1),\\
y_5 &= p^2(y_2+1) + p(1-p)(y_4+1)\\
&\quad + p(1-p)(y_6+1) + (1-p)^2(y_7+1),\\
y_6 &= p^2(y_1+1) + p(1-p)(y_4+1)\\
&\quad + p(1-p)(y_5+1) + (1-p)^2(y_7+1),\\
y_7 &= p^3 + 3p^2(1-p) + p^2(1-p)(y_1+y_2+y_3)\\
&\quad + 3p(1-p)^2 + p(1-p)^2(y_4+y_5+y_6)\\
&\quad + (1-p)^3(y_7+1).
\end{aligned} \tag{6}$$

With Eq. (6) we obtain the solutions $y_1 = y_2 = y_3 = \frac{1+p+2p^4-p^2-p^5}{p^3(1+2p^2-2p-p^3)}$, $y_4 = y_5 = y_6 = \frac{1+p+3p^4-p^2-2p^5}{p^3(1+2p^2-2p-p^3)}$, and $y_7 = \frac{1+3p+3p^2}{p^3}$. For the case of $p = 1/2$, we have $y_1 = y_2 = y_3 = 86/3$, $y_4 = y_5 = y_6 = 88/3$, and $y_7 = 26$. As y_7 represents the case of initially activated m nodes, we have $\langle T\rangle = y_7 = 26$, which is also consistent with Fig. 7(f).

We notice from these two cases of $m = 2$ and 3 that their solutions y_i depend only on the numbers of the initially activated nodes. In the case of $m = 2$, the initial activation states of 01 and 10 have the same $y_1 = y_2$. While in the case of $m = 3$, the initial activation states of 001, 010, and 100 have the same $y_1 = y_2 = y_3$ and the initial activation states of 011, 101, and 110 have the same $y_4 = y_5 = y_6$. Based on this observation, we now derive a general formula for the average lifetime $\langle T\rangle$ with different m. For this purpose, we let the number of initially activated nodes represent the state of system. Table III shows the probabilities for each initial activation, where the first line represents the m initial activation states, the first column denotes the $m+1$ possible outputs, and $q(i, j)$ represents the probability from j initially activated nodes to become i activated nodes at the next step.

For each specific m, the expression of $q(i, j)$ can be determined as in Tables I and II. Then we can obtain its $\langle T\rangle$ by the similar derivative processes as in the cases of $m = 2$ and 3. We find that $\langle T\rangle = (4p^3 + 6p^2 + 4p + 1)/p^4$ for the case of Fig. 7(c) with $m = 4$, $\langle T\rangle = (5p^4 + 10p^3 + 10p^2 + 5p + 1)/p^5$ for the case of Fig. 7(d) with $m = 5$, and so on. It is very interesting to note that we find that all the formulas of $\langle T\rangle$ for different m can be unified into

$$\langle T\rangle = \sum_{i=1}^{m} C_m^i p^{m-i}/p^m. \tag{7}$$

It gives $\langle T\rangle = 80$ for $m = 4$, $\langle T\rangle = 242$ for $m = 5$, and so on, when $p = 1/2$. The "triangles" in Fig. 7(f) show the theoretical results for $m = 1, 2, \ldots, 15$. Comparing them with the corresponding "circles" from simulations, we see that they are are very consistent.

Moreover, because of $p < 1$, the numerator of Eq. (7) will be $O(1)$, thus $\langle T\rangle$ is proportional to $1/p^m$. We have $\langle T\rangle \sim 2^m$ when $p = 1/2$, which is just what we have observed in Fig. 7(f).

IV. DISCUSSION AND CONCLUSIONS

So far, we have discussed the multiscaled rhythms of RSNs from the angle of microstates. These results are based on the cognitive brain network, but they can be extended to other brain networks such as the brain network of the cerebral cortex [22,47] and personalized brain networks [48]; see the

TABLE III. The m initial activation states vs their outputs.

State	1	2	$\cdots$	$m-1$	m
0	$q(0,1)$	$q(0,2)$	$\cdots$	$q(0,m-1)$	$q(0,m)$
1	$q(1,1)$	$q(1,2)$	$\cdots$	$q(1,m-1)$	$q(1,m)$
2	$q(2,1)$	$q(2,2)$	$\cdots$	$q(2,m-1)$	$q(2,m)$
$\vdots$	$\vdots$	$\vdots$	$\vdots$	$\vdots$	$\vdots$
$m-1$	$q(m-1,1)$	$q(m-1,2)$	$\cdots$	$q(m-1,m-1)$	$q(m-1,m)$
m	$q(m,1)$	$q(m,2)$	$\cdots$	$q(m,m-1)$	$q(m,m)$

SM [34] for details. Thus, these findings may be general in brain networks. As the brain is usually considered to work at the edge of a critical point, our results may reveal some principles of cognitive functions in the following aspects: (1) the TLSOP contains one or a few core networks, which is the reason for the multiscaled rhythms of RSNs. For example, Fig. 1(b) contains all the core networks of Figs. 1(c)–1(f). However, the core networks of Figs. 1(c)–1(f) may not be the whole in Fig. 1(b). (2) The rhythm of a core network is determined by a weighted or ensemble average on all its microstates, i.e., some microstates are dominant. (3) The return times of microstates satisfy the Weibull distribution, i.e., not a purely power-law or exponential distribution but in between. It is well known that power-law distributions are usually connected with the criticality of the brain, while exponential distributions are related to random processes [49,50]. This finding of a Weibull distribution implies that a TLSOP depends on both the criticality of the brain and noise, which is consistent with the features of RSNs [13,51].

In conclusion, based on the fact that biological rhythms are usually related to finite time series or transient processes, we systematically study TLSOPs and their mechanisms. We first present a simplified reaction-diffusion model and find that it can reproduce various TLSOP patterns, indicating that the TLSOP mechanisms may be very simple. Then we make further studies step by step. The first step is how to identify the individual rhythms from multiscaled TLSOPs. To solve this problem, we present an approach of dominant activation paths and find the core network for each individual rhythm. Moreover, based on this approach, we show a way to implement the switching between different TLSOP rhythms . The second step is to study the statistics of TLSOP microstates. For this purpose, we present a return-loop approach and find that the return times of microstates satisfy the Weibull distribution, marking the feature of nonequilibrium state. The third step is to check the discovered Weibull distribution with the real data of RSNs. To do it, we consider the cases of both fMRI and EEG data and show that they do satisfy the Weibull distribution, where a byproduct, i.e., the shifting window approach, is presented. In the final step, we present a brief theory to explain the dependence of lifetimes on the sizes of core networks, based on the complete graphs.

ACKNOWLEDGMENTS

This work was partially supported by the NNSF of China under Grants No. 11835003, No. 82161148012, and No. 12175070, and the "Technology Innovation 2030–Major Projects" on brain science and brain-like computing of the MST of China (Grant No. 2021ZD0202600). M.K. was supported by the Wellcome Trust (102037), Engineering and Physical Sciences Research Council (NS/A000026/1, EP/N031962/1), Medical Research Council (MR/T004347/1), and Guangci Professorship Program of Rui Jin Hospital (Shanghai Jiao Tong University).

[1] D. S. Bassett and O. Sporns, Network neuroscience, Nat. Neurosci. **20**, 353 (2017).
[2] A. Avena-Koenigsberger, B. Misic, and O. Sporns, Communication dynamics in complex brain networks, Nat. Rev. Neurosci. **19**, 17 (2018).
[3] A. Fornito, A. Zalesky, and M. Breakspear, The connectomics of brain disorders, Nat. Rev. Neurosci. **16**, 159 (2015).
[4] M. Bibireata, V. M. Slepukhin, and A. J. Levine, Dynamical phase separation on rhythmogenic neuronal networks, Phys. Rev. E **101**, 062307 (2020).
[5] G. Buzsaki and A. Draguhn, Neuronal oscillations in cortical networks, Science **304**, 1926 (2004).
[6] G. Buzsaki and B. O. Watson, Brain rhythms and neural syntax: Implications for efficient coding of cognitive content and neuropsychiatric disease, Dialogues Clin. Neurosci. **14**, 345 (2012).
[7] V. Piai, K. L. Anderson, J. J. Lin, C. Dewar, J. Parvizi, N. F. Dronkers, and R. T. Knight, Direct brain recordings reveal hippocampal rhythm underpinnings of language processing, Proc. Natl. Acad. Sci. USA **113**, 11366 (2016).
[8] M. C. M. Bastiaansen, M. Van Der Linden, M. Ter Keurs, T. Dijkstra, and P. Hagoort, Theta responses are involved in lexical–semantic retrieval during language processing, J. Cogn. Neurosci. **17**, 530 (2005).
[9] M. Marko, B. Cimrova, and I. Riecansky, Neural theta oscillations support semantic memory retrieval, Sci. Rep. **9**, 17667 (2019).
[10] M. D. Sacchet *et al.*, Attention drives synchronization of alpha and beta rhythms between right inferior frontal and primary sensory neocortex, J. Neurosci. **35**, 2074 (2015).
[11] A. von Stein, P. Rappelsberger, J. Sarnthein, and H. Petsche, Synchronization between temporal and parietal cortex during multimodal object processing in man, Cereb. Cortex **9**, 137 (1999).
[12] A. J. K. Phillips and P. A. Robinson, A quantitative model of sleep-wake dynamics based on the physiology of the brainstem ascending arousal system, J. Biol. Rhythms **22**, 167 (2007).
[13] I. P. Ipiña *et al.*, Modeling regional changes in dynamic stability during sleep and wakefulness, NeuroImage **215**, 116833 (2020).

[14] C. E. Carr, Processing of temporal information in the brain, Annu. Rev. Neurosci. **16**, 223 (1993).

[15] D. V. Buonomano and W. Maass, State-dependent computations: Spatiotemporal processing in cortical networks, Nat. Rev. Neurosci. **10**, 113 (2009).

[16] G. Mongillo, O. Barak, and M. Tsodyks, Synaptic theory of working memory, Science **319**, 1543 (2008).

[17] Y. Mi *et al.*, Long-period rhythmic synchronous firing in a scale-free network, Proc. Natl. Acad. Sci. USA **110**, 4931 (2013).

[18] K. Xu, X. Zhang, C. Wang, and Z. Liu, A simplified memory network model based on pattern formations, Sci. Rep. **4**, 7568 (2014).

[19] K. Xu, W. Huang, B. Li, M. Dhamala, and Z. Liu, Controlling self-sustained spiking activity by adding or removing one network link, Europhys. Lett. **102**, 50002 (2013).

[20] A. Roxin, H. Riecke, and S. A. Solla, Self-Sustained Activity in a Small-World Network of Excitable Neurons, Phys. Rev. Lett. **92**, 198101 (2004).

[21] K. Bansal *et al.*, Cognitive chimera states in human brain networks, Sci. Adv. **5**, eaau8535 (2019).

[22] C. J. Honey, O. Sporns, L. Cammoun, X. Gigandet, J. P. Thiran, R. Meuli, and P. Hagmann, Predicting human resting-state functional connectivity from structural connectivity, Proc. Natl. Acad. Sci. USA **106**, 2035 (2009).

[23] O. Kinouchi and M. Copelli, Optimal dynamical range of excitable networks at criticality, Nat. Phys. **2**, 348 (2006).

[24] N. Brunel and V. Hakim, Fast global oscillations in networks of integrate-and-fire neurons with low firing rates, Neural Comput. **11**, 1621 (1999).

[25] A. Bashan, R. P. Bartsch, J. W. Kantelhardt, S. Havlin, and P. Ch. Ivanov, Network physiology reveals relations between network topology and physiologic function, Nat. Commun. **3**, 702 (2012).

[26] M. Massimini, F. Ferrarelli, R. Huber, S. K. Esser, H. Singh, and G. Tononi, Breakdown of cortical effective connectivity during sleep, Science **309**, 2228 (2005).

[27] G. Buzsaki, *Rhythms of the Brain* (Oxford University Press, New York, 2006).

[28] C. J. Stam, B. F. Jones, G. Nolte, M. Breakspear, and P. Scheltens, Small world networks and functional connectivity in Alzheimer's disease, Cereb. Cortex **17**, 92 (2007).

[29] M. Chavez, M. Valencia, V. Navarro, V. Latora, and J. Martinerie, Functional Modularity of Background Activities in Normal and Epileptic Brain Networks, Phys. Rev. Lett. **104**, 118701 (2010).

[30] S. F. Muldoon *et al.*, Stimulation-based control of dynamic brain networks, PLoS Comput. Biol. **12**, e1005076 (2016).

[31] Q. Shen and Z. Liu, Remote firing propagation in the neural network of *C. elegans*, Phys. Rev. E **103**, 052414 (2021).

[32] Z. Wang and Z. Liu, Effect of remote signal propagation in an empirical brain network, Chaos **31**, 063126 (2021).

[33] M. Kaiser, M. Gorner, and C. C. Hilgetag, Criticality of spreading dynamics in hierarchical cluster networks without inhibition, New J. Phys. **9**, 110 (2007).

[34] See Supplemental Material at http://link.aps.org/supplemental/10.1103/PhysRevResearch.4.023076 for TLSOPs and distributions of return-times in other subjects, the Brody distributions of return-times for all subjects, the case of a larger cerebral cortex network, the case of personalized medium-size networks, fMRI and EEG data including the shifting window analysis, and non-resting-state fMRI and EEG data.

[35] https://zenodo.org/record/2590869.

[36] J. D. Power *et al.*, Functional network organization of the human brain, Neuron **72**, 665 (2011).

[37] Y. Qian, X. Huang, G. Hu, and X. Liao, Structure and control of self-sustained target waves in excitable small-world networks, Phys. Rev. E **81**, 036101 (2010).

[38] X. H. Liao, Y. Qian, Y. Mi, Q. Z. Xia, X. Q. Huang, and G. Hu, Oscillation sources and wave propagation paths in complex networks consisting of excitable nodes, Front. Phys. **6**, 124 (2011).

[39] P. Bak, C. Tang, and K. Wiesenfeld, Self-Organized Criticality: An Explanation of the $1/f$ Noise, Phys. Rev. Lett. **59**, 381 (1987).

[40] M. A. Muñoz, Colloquium: Criticality and dynamical scaling in living systems, Rev. Mod. Phys. **90**, 031001 (2018).

[41] J. W. J. L. Wang, F. Lombardi, X. Zhang, C. Anaclet, and P. Ch. Ivanov, Non-equilibrium critical dynamics of bursts in θ and δ rhythms as fundamental characteristic of sleep and wake microarchitecture, PLoS Comput. Biol. **15**, e1007268 (2019).

[42] J. S. Damoiseaux *et al.*, Consistent resting-state networks across healthy subject, Proc. Natl. Acad. Sci. USA **103**, 13848 (2006).

[43] D. C. Van Essen, S. M. Smith, D. M. Barch, T. E. Behrens, E. Yacoub, K. Ugurbil, and WU-Minn HCP Consortium, The WU-Minn Human Connectome Project: An overview, NeuroImage **80**, 62 (2013).

[44] V. M. Eguíluz, D. R. Chialvo, G. A. Cecchi, M. Baliki, and A. V. Apkarian, Scale-Free Brain Functional Networks, Phys. Rev. Lett. **94**, 018102 (2005).

[45] T. Watanabe *et al.*, A pairwise maximum entropy model accurately describes resting-state human brain networks, Nat. Commun. **4**, 1370 (2013).

[46] R. Mehraram *et al.*, Weighted network measures reveal differences between dementia types: An EEG study, Hum. Brain. Mapp. **41**, 1573 (2020).

[47] P. Hagmann, L. Cammoun, X. Gigandet, R. Meuli, C. J. Honey, J. V. Wedeen, and O. Sporns, Mapping the structural core of human cerebral cortex, PLoS Biol. **6**, e159 (2008).

[48] K. Bansal, J. D. Medaglia, D. S. Bassett, J. M. Vettel, and S. F. Muldoon, Data-driven brain network models differentiate variability across language tasks, PLoS Comput. Biol. **14**, e1006487 (2018).

[49] A. J. Fontenele *et al.*, Criticality between Cortical States, Phys. Rev. Lett. **122**, 208101 (2019).

[50] G. Deco, G. Tononi, M. Boly, and M. L. Kringelbach, Rethinking segregation and integration: Contributions of whole-brain modelling, Nat. Rev. Neurosci. **16**, 430 (2015).

[51] G. Deco, A. Ponce-Alvarez, D. Mantini, G. L. Romani, P. Hagmann, and M. Corbetta, Resting-state functional connectivity emerges from structurally and dynamically shaped slow linear fluctuations, J. Neurosci. **33**, 11239 (2013).